Ultra-Fast Magnetic Resonance Imaging Sequences

Afonso C. Silva* and Irving J. Lowe†
Pittsburgh NMR Center for Biomedical Research
Carnegie Mellon University, Pittsburgh, Pennsylvania 15.213

Received September 23, 1995

In conventional magnetic resonance imaging (MRI), the scan times are usually long due to the necessity of a waiting period of tlie order of the relaxation time constant T_1 between the successive excitations required for sampling the data. For time dependent phenomena, such as physiological processes and sample motion, faster acquisition times are desirable. A number of ultra-fast MRI sequences have been proposed over the last two decades that greatly reduce the acquisition time either by repeatedly scanning the magnetization using a single excitation or by using multiple low flip-angle excitation schemes. The purpose of this work is to provide the reader with a qualitative review of some of these sequences in terms of both their implementation and hardware requirements, as well as their useful range of applications.

I. Introduction

Magnetic resonance imaging (MRI) has established itself as a very useful non-invasive imagingmodality. Its main applications are found in medicine, not only as a very powerful tool for visualization of tissue anatomy and structure, but also in the determination of organ viability, metabolism, and function. MRI has further found numerous applications in physics, biology, chemistry, biochemistry and materials science as well. However, conventional MRI is a slow imaging technique compared to ultra-sound or to X-ray computed tomography, for example. The long scan times of MRI (on the order of 5-10 minutes to produce a conventional MR image) effectively decrease its potential range of applications. For example, the quality of tlie image can be greatly affected by motion of the sample during acquisition time. Many normal physiological processes, like respiration, blood flow pulsation, and peristalsis can cause substantial artifacts in the image, like blurring and ghost artifacts. Moreover, there are rnany events, like the motion of the heart walls, or the study of flow dynamics, that can only be followed if the acquisition time is fast compared those events.

In this review, MRI techniques that greatly reduce scan times are discussed as a way to extend the range of applications of conventional MRI. These techniques are referred to as ultra-fast imaging sequences, and they are able to produce images in times typically less than 100 ms. In order to give the reader a better understanding of how the ultra-fast imaging sequences work, the first section of this paper describes how the data are typically acquired in conventional MRI. In particular, it is shown that an image, namely the nuclear spin density distribution in two-dimensional spatial coordinates, can be obtained by taking a two-dimensional Fourier transform of the data acquired in the reciprocal space, which is named k-space in MRI. Using the k-space formalism, the different types of imaging sequences can be described in terms of their trajectories through k-space. Section II presents two types of ultra-fast imaging sequences that use a single excitation to scan k-space, namely Echo-Planar Imaging (EPI) and Spiral-Scan Imaging. Section III discusses sequences

*Biomedical Engineering Program, Carnegie Mellon University, Pittsburgh, Pennsylvania, 15213
†Department of Physics and Astronomy, University of Pittsburgh, Pittsburgh, Pennsylvania 15260

that use multiple excitation: FLASH, BURST, DUFIS, OUFIS and RUFIS. Finally, section IV contains a qualitative discussion of the applications of ultra-fast imaging sequences, and surveys the prospects of ultra-fast MRI.

II. Conventional MRI

The Larmor speed w of a nuclear spin with a magnetogyric ratio 7 in a magnetic field B_0 is given by $\omega_0 = \gamma B_0$. MRI is based upon encoding the resonance frequency of the nuclear spins according to their spatial coordinates. This is done with the aid of linear varying magnetic fields (field gradients), that are applied to the sample along with the much larger polarizing magnetic field B_0. If a fixed linear gradient G is applied to a sample, the local resonance frequency of tlie nuclear spins can be defined as a function of the spins spatial coordinate r as $\omega(\mathbf{r}) = \gamma B_0 + \gamma \mathbf{G} \cdot \mathrm{r}$. Neglecting transverse relaxation, the NMR signal from the nuclear spins located at position r in a small element of volume dV of the sample is given by

$$dS(t) = A\rho(\mathbf{r})dV \exp[i(\gamma B_0, +\gamma \mathbf{G} \cdot \mathbf{r})t] , \qquad (1)$$

where A is a constant of proportionality and $\rho(\mathbf{r})$ is tlie nuclear spin density function.

Relative to the reference frequency $\omega_0 = \gamma B_0$, the total signal amplitude will be given by

$$S(t) = A \int\int\int \rho(\mathbf{r}) \exp[i\gamma \mathbf{G} \cdot \mathbf{r}t] dV \qquad (2)$$

Equation (2) shows that the relation between the acquired signal $S(t)$ and the nuclear spin density function $\rho(\mathbf{r})$ has the form of a Fourier transforrn. This relation can be more easily seen by using the concept of k-space[1], through the use of a reciproca1 space vector k defined as

$$\mathrm{k} = \frac{1}{2\pi}\gamma \int_0^t \mathbf{G} d\tau \qquad (3)$$

It is clear from Eq. (3) that k-space may be traversed by moving either in time and/or in gradient strength and direction. Using this formalism, Eq. (2) may be rewritten as a pair of the Fourier transform and its inverse, namely

$$\begin{aligned} S(\mathbf{k}) &= A \int\int\int \rho(\mathbf{r}) \exp[i2\pi \mathbf{k} \cdot \mathbf{r}] dV \\ \rho(\mathbf{r}) &= A \int\int\int S(\mathbf{k}) \exp[i2\pi \mathbf{k} \cdot \mathbf{r}] d\mathbf{k} \end{aligned} \qquad (4)$$

Equation (4) shows that an image of the nuclear spin density function can be obtained by taking the Fourier transform of the NMR signal acquired in the k-space domain. In a three-dimensional sample, the nuclear spins contained in a slice of thickness δ are selectively excited to produce NMR signals only across the slice. The reconstruction is then performed in the two dimensions of the slice plane by means of a two-dimensional Fourier transform. For example, for a slice of thickness δ cut perpendicular to the z direction at z_0, the signal is given by:

$$S(k_x, k_y) = A \int_{z_0-\delta/2}^{z_0+\delta/2} \left[\int_{-\infty}^{\infty} \int_{-\infty}^{\infty} \rho(x, y, z) \exp\{i2\pi (k_x x + k_y y)\} dx dy \right] dz \qquad (5)$$

The outer integral in Eq. (5) represents only an averaging across the slice, and can be conveniently ignored so that reconstruction of the averaged nuclear spin area density function $\rho(x, \mathrm{y}, z_0)$ into an image is performed by taking the two-dimensional inverse Fourier transform given by:

$$\rho(x, y, z_0) = \int_{-\infty}^{\infty} S(k_x, k_y) \exp[-i2\pi (k_x x + k_y y)] dx dy \qquad (6)$$

When tlie signal is sampled in the presence of a fixed

gradient, a single line in tlie direction of the gradient is scanned in L-space. It is usual to orient this line along one of tlie Cartesian axis and use tlie term 'frequency-encoding' or 'read' direction for that particular axis. The intercept of this line along tlie ortliogonal axis can be varied by applying an ortliogonal field gradient for a fixecl period of time before tlie sampling begins. The resulting phase-modulation of tlie signal along the orthogonal axis names this a i s tlie 'phase-encoding' direction. In conventional MRI scliemes, a. total of N_r, points are acquired in tlie read direction along a single line in L-space and tlie experiment is repeatecl N_p times using different phase-encoding gradient amplitudes to complete the k-space raster. Tlie echo time TE that elapses between tlie onset of tlie slice selective excitation and tlie center of tlie eclio in k-space is usually of tlie order of several milliseconds. After tlie acquisition of a line along the frequency encoding direction in b-space, a waiting period is observecl to allow for partial longitudinal (T_1) relaxation of tlie nuclear spins magnetization. Therefore, the repetition time T R between two consecutive excitation steps is usually of tlie order of T_1. This forces the total acquisition time for a single image to be on the order of $N_p T_1$, a time that can typically range from about 2 minutes up to around 15 minutes.

Basecl on the k-space formalism presented above, Fig. 1 shows tlie timing diagram and tlie k-space trajectories of two conventional ways of producing a two-climensional MR Image. Fig. 1A describes tlie gradient-echo imaging sequence. After tlie longitudinal magnetization of the spins contained in a given slice of the sample is brought into tlie transverse plane by ineaiis of a slice-selective RF pulse, the phase-encoding and read gradients are applied for a short period of time to move tlie transverse magnetization to the left-edge of k-space. At this point the phase-encoding graclient is switched off and tlie polarity of tlie read gradient is inverted, causing tlie magnetization to evoive in k-space in tlie read direction while the signal is being sainplecl. The reversal of the read graclient refocus the spread of Larmor frequencies along the read direction. It should be noticed, however, that only those precessions caused by the initial application of the read gradient are re-

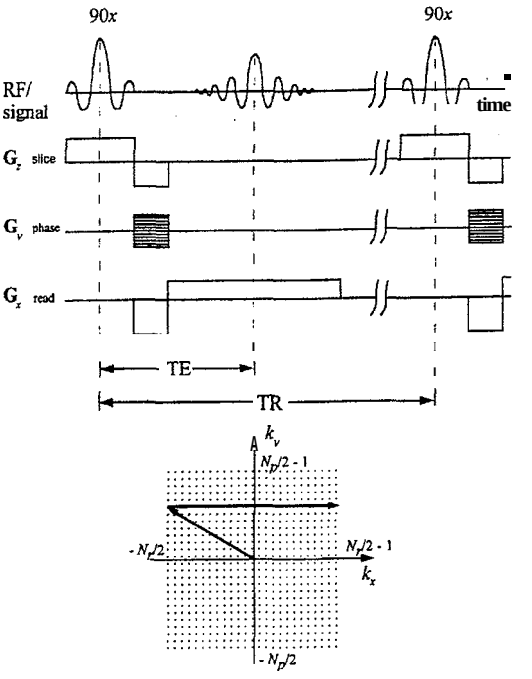

Figure 1A

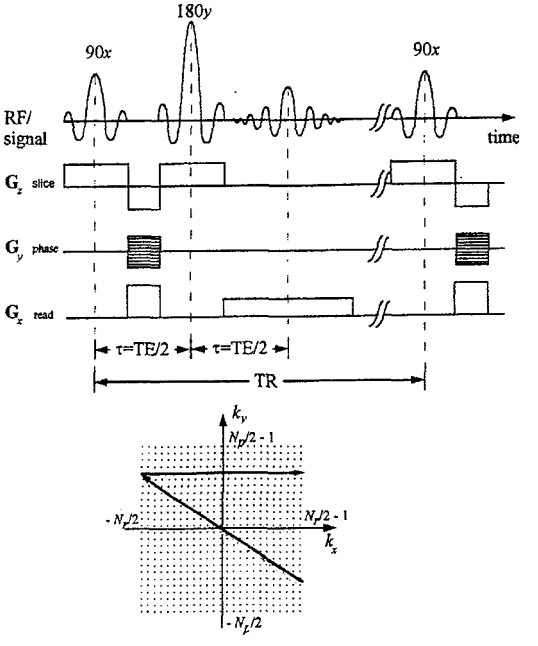

Figure 1B

i r e 1. (A) Gradient-echo imaging sequence. After tlie slice-selective excitation RF pulse, the transverse magnetization is phase-encoded and brought to the left-edge of k-space by a negative preciirsor read gradient. Tlie read gradient is then reversed and N_r points along a single line in k-space are acquired. This process is repeated at a rate given by the repetition time TR using increasing values for tlie phase-encoding gradient until N_p lines have been acquired. (B) Spin-warp imaging sequence. A precursor read gradient is applied together with the phase-encoding gradient to make the magnetization evolve to the right side of k-space. A 180° RF pulse is then used to invert the phase sliifts of the magnetization, which is acquired in tlie presente of tlie read gradient.

focussed upon gradient reversal. Local field inhomogeneities, chemical shift and susceptibility variations cause phase shifts which are not refocussed, so that the gradient-echo sequence is subject to T_2^* relaxation in which both homogeneous and inhomogeneous broadening are involved. Fig. 1B describes the spin-warp (spin-echo) imaging sequence. As with the gradient-echo imaging sequence shown in Fig. 1A, the phase-encoding and read gradients are applied for a short period of time after slice-selection to cause k-space evolution. However, a 180° RF pulse is placed at a time τ after the 90° RF pulse in the spin-warp sequence to invert the phase shifts associated with the precursor gradient pulses. This way, both homogeneous as well as inhomogeneous broadening are refocussed at a time 2τ after the 90° RF pulse, at the center of the echo. so that the signal in the spin-echo imaging sequence is subject only to T_2 relaxation.

The contrast obtained in the image is given by a balance of T_2 and T_1 weightings of the signal, which are controlled by a choice of the TE and the TR times used. The use of shorter TR times may lead to excessive T_1 attenuation of the signal, compromising the signal-to-noise ratio (SNR) and therefore the sensitivity and quality of the experiment, or impose excessive T_1 weighting of the image. In order to reduce the total acquisition time significantly, the TR time has to be greatly reduced, or eliminated. This has to be accomplished, however, without inducing T_1 signal attenuation. One way to scan k-space rapidly is to use a single excitation period and recall the resulting transverse magnetization over and over until all the necessary $N_r N_p$ points in k-space have been collected. Examples of techniques that use this method are Echo-Planar Imaging and Spiral-Scan Imaging, and will be described in section II. A different way of producing an ultra-fast MR Image is to use low flip angle excitations to produce a string of echoes along the read direction and to phase encode each echo in the orthogonal direction so that k-space is entirely covered. Examples of sequences that use this idea are FLASH, BURST, DUFIS, OUFIS and RUFIS, which will be discussed in section III.

II. Single excitation ultra-fast imaging sequences

II.1 Echo-planar imaging sequence

The transverse magnetization produced by a single slice-selective excitation can be used to scan k-space entirely, as long as the scan is fast compared to the sample's transverse relaxation rate T_2. This idea, due to Mansfield[2] and co-workers[3–5], gave origin to the Echo-Planar Imaging (EPI) sequence. Fig. 2 shows the timing diagram and the k-space trajectories of the EPI sequence. The transverse magnetization created by a single slice-selective 90° RF pulse is brought to one corner of k-space by applying the phase-encoding and read gradients for a short period of time. The phase-encoding gradient is then shut-off while the read gradient is reversed and an echo signal is sampled in a similar manner to the gradient-echo imaging sequence shown presented in section I. Therefore, the EPI sequence shown in Fig. 2 is also called gradient-echo EPI. After the acquisition of a line along the read direction in k-space, the phase-encoding gradient is 'blipped' so as to cause orthogonal evolution of the magnetization to the next line. The read gradient is then reversed again and a new line is acquired, this time in the opposite direction with respect to the previous line. This process of blipping the phase-encoding gradient and inverting the polarity of the read gradient is repeated until all N_p data lines have been acquired. The entire data set is acquired within a single image acquisition window W. In the gradient-echo EPI sequence, the effective echo time TE is counted as the time that elapses from the center of the RF pulse to the time when the center of k-space is scanned. The repetition time TR is now the time elapsed between two consecutive images, and can be arbitrarily long. In order to correct for the opposite scan direction due to the negative polarity of the read gradient, the even echoes have to be time-reversed prior to the Fourier transform reconstruction.

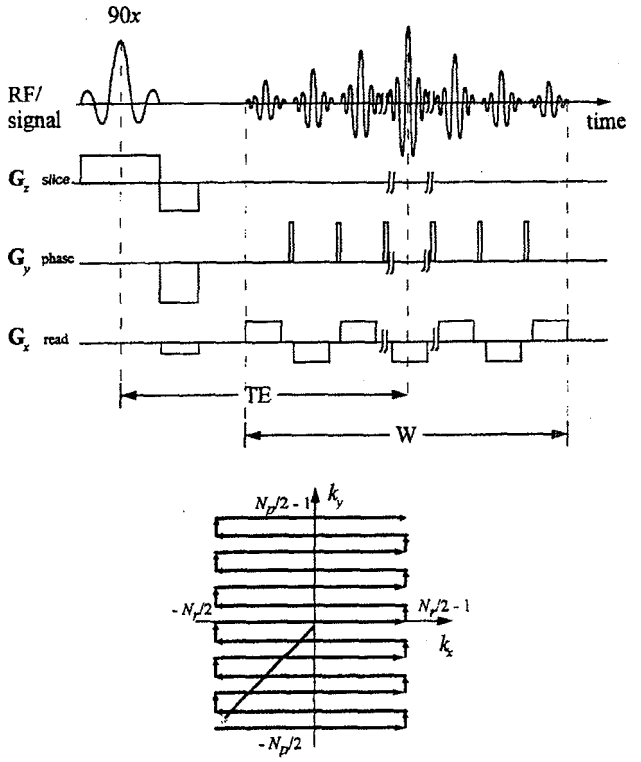

Figure 2. Eclio-Planar Imaging (EPI) Sequence. The magnetization created by the slice-selective 90° RF pulse is recalled N_p times by alternating the polarity of tlie read gradient, so that all lines in H-space are acquired witliin a single image acquisition window W. Each individual echo is phase-encoded by blipping the phase-encoding gradient prior to collection of the echo. Because consecutive lines in H-space are sampled in opposite directions, the alternate data lines have to be reversed prior to the Fourier transform reconstruction.

As with the gradient-echo imaging sequence, the gradient-echo EPI sequence is also subject to T_2^* attenuation. In particular, because TR can be arbitrarily long, the image can be characterized by true T_2^* contrast. As a method of reducing the effects of field inhomogeneities in this sequence, a spin-echo version of EPI was proposed by Rzedzian and Pykett[6,7] which used a 180° RF pulse placed at a time τ after the slice-selective 90° RF pulse to generate a spin-echo of the transverse magnetization. In this scheme, illustrated in Fig. **3,** the timing is adjusted so that the center of the echo train TE (which is also the center of H-space) occurs at time 2τ from the 90° RF pulse. All inhomogeneous broadening is refocussed at time 2τ, making the sequence somewhat less sensitive to off-resonance effects. This is an advantage in many applications, but with the gradient-echo version of EPI, the absence of the 180° RF pulse allows the echo-train to be moved closer to the slice-selective excitation pulse for a shorter effective echo time TE.

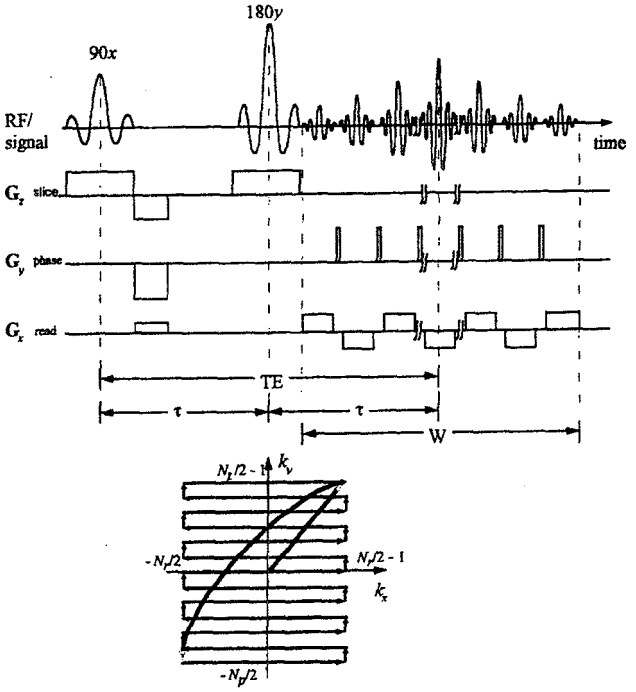

Figure 3. Spin-Echo EPI. A 180° RF pulse is placed at a time r after the slice-selective 90° excitation pulse to refocus inhomogeneous broadening. The timing is adjusted so that the center of the acquisition window (center echo) is positioned at time 2τ after the slice-selective RF pulse. the amplitude modulation of the echoes is due to the phase-encoding gradient blips.

The total scan time in either one of the versions of the EPI-sequence depends on the selected effective TE time and on the time length of the acquisition window, W. Complete images with matrix data sizes up to 128 x 128 pixels have been acquired in times of the order of 25-100 ms[4-8].

A number of different issues have to be analyzed when considering the practical limitations of the EPI sequence. One of the most common difflculties found in the implementation of the sequence in standard commercial MRI scanners concerns hardware requirements. EPI demands a scanner equipped with gradient coils capable of generating over 1 G/cm with slew rates faster than 200 μs/G/cm, and a fast A/D converter capable of handling bandwidths well in excess of 250 kHz. For example, the images acquired by Pykett and Rzedzian in [7] have a field-of view (FOV) of 51.2 × 25.6 cm^2, a matrix data size of 128 x 64 pixels and an acquisition window W = 26 ms. Assuming the time required

for a phase-encoding gradient blip is about 50 ps, each echo is acquired in approximately 357 μs or at a sampling rate of 2.8 μs/data point, which corresponds to a sampling bandwidth of about 360 kHz. Assuming the read gradient is subject to a ramp time of 100 μs, which is typically about 5 times less than in commercial scanners, the peak gradient value is equal to 2.1 G/cm [9]. Çmaller FOVs require even larger gradients. Another problem faced in the implementation of the EPI sequence is the presence of artifacts induced by eddy-currents associated with the fast switching of the gradients[3]. In fact, a key factor in the successful implementation of EPI has been the development of screened gradient coils[10–12]. These coils enable fast current switching without inducing the associated eddy-currents.

The spatial resolution in a conventional MRI sequence is affected by the number of data points acquired during the decay of an echo and by intravoxel inhomogeneities. In EPI, the same principles dictating spatial resolution are valid. The maximum spatial resolution that can be obtained with EPI is limited mainly in the phase-encoding direction by T_2 and off-resonance effects such as rnagnetic susceptibility and chemical shift in the sample with respect to the sampling bandwidth. In particular, there are two additional problems caused by field inhomogeneities: (a) miscentering of the echoes, and (b) spatially varying phase shifts. Miscentering of the echoes occurs if the read gradients are not adjusted properly, or if a linear component of field inhomogeneity exists along the read direction. Either condition will shift the center of each echo from the center of its corresponding readout period, resulting in geometric artifacts and ghosting. Spatially varying phase shifts may cause distortions such as shifting, magnification and scaling of the image in the phase encoding direction.

11.2 Spiral-scan imaging

The Spiral-Scan Imaging sequence was proposed in 1986 by Ahn, Kim and Cho[13] as an alternative to EPI. The technique avoids EPI's troublesome gradient switching, and also its non-isotropic resolution caused by different T_2 weigliting in the read and phase-encoding directions. The sequence is based on covering k-space in a circularly symmetric spiral scan, as shown in Fig. 4. The k-space position of the magnetization at a time t after beginning acquisition can be described in polar coordinates as:

$$k_x = A\theta(t)\cos\theta(t) \quad (7)$$

$$k_y = A\theta(t)\sin\theta(t) \quad (8)$$

where A is a constant. The time dependence of θ determines the rate of traversal of the spiral trajectory. Three types of bidimensional spiral trajectories have been proposed in the literature: (i) constant angular velocity spirals[13], which allow the image to be reconstructed by means of a filtered back projection algorithm, (ii) constant slew rate with negligible acceleration spirals[14], that have mathematically closed form gradients at large radii in k-space, and (iii) maximum gradient spirals[15], that have the shortest readout time. In the particular case of constant angular velocity spirals,

$$\theta(t) = \xi t \quad (9)$$

where ξ is a constant corresponding to the angular velocity of the spiral. In this case, the gradients $G_x(t)$ and G_y(t) can be calculated as:

$$G_x(\mathrm{t}) = \frac{2\pi}{\gamma}\frac{\partial k_x(t)}{\partial t} = \frac{2\pi}{\mathrm{Y}}A\xi[\cos\xi t - \xi t\sin\xi t]$$

$$G_y(t) = \frac{2\pi}{\gamma}\frac{\partial k_y(t)}{\partial t} = \frac{2\pi}{\mathrm{Y}}A\xi[\sin\xi t - \xi t\cos\xi t] \quad (10)$$

The gradients $G_x(t)$ and $G_y(t)$ are then sinusoidal signals with linearly increasing amplitude as a function of time, as shown in Fig. 4. The spatial resolution obtained with the Spiral-Scan sequence is given by the number of turns in the spiral, N_r, and the number of points acquired per turn, N_θ. The radial and angular increments in k-space, Ak, and Δk_θ in Fig. 4, respectively, are related to the sampling interval AT according to:

$$\mathrm{Ak}, = a\xi N_\theta \Delta T = \frac{2\pi}{2N_r\Delta r}$$

$$\Delta k_\theta = \xi\Delta T = \frac{2\pi}{2N_\theta} \quad (11)$$

where Ar is the image resolution in the spatial domain, and the last terms in Eq. (11) correspond to the

Nyquist sampling rate. From Eq. (11), tlie constants A and ξ can be determined as:

$$A = \frac{1}{2N_r\Delta r}$$
$$\xi = \frac{2\pi}{N_\theta \Delta T} \qquad (12)$$

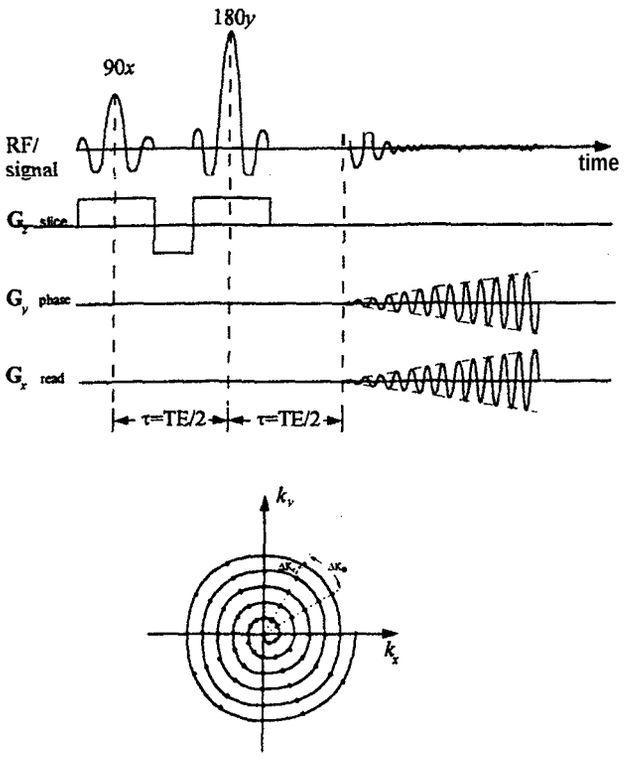

Figure 4. Spiral-Scan Imaging. Tlie transverse magnetization created by a 90° RF pulse is refocussed by a 180° RF pulse and acquisition starts at time TE $= 2\tau$, when tlie gradients G_x and G_y. are turned on. These gradients are sinusoidal signals with amplitude linearly increasing as a function of time, determining that k-space is scanned along a spiral trajectory.

The total acquisition window W and tlie maximum gradient amplitude $G_{\max}$ are:

$$W = N_r N_\theta \Delta T$$
$$G_{\max} = \frac{2\pi}{\gamma} A\xi^2 W = \frac{4\pi^3}{\gamma N_\theta \Delta T} \qquad (13)$$

Some advantages of tlie Spiral-Scan sequence includes low sensitivity to motion and to flow artifacts[16,17]. However, due to the long readout time W given by Eq. (13), Spiral-Scan suffers from blurring caused by field inhomogeneities, cliemical shift or susceptibility gradients[18–20]. This blurring is usually worse tlian the effect of T_2^* decay, so that the best approach for Spiral-Scan Imaging is to use the maximum gradient approach that minimizes the readout time. The gradient waveforrns can be optimized with respect to blurring from off-resonance effects by minimizing the readout time[21]. This is achieved by maximizing tlie gradient amplitude during the scan to reach tlie edge of k-space in the shortest time possible.

III. Multiple excitation ultra-fast imaging sequences

In the previous section ultra-fast MRI sequences that use a single excitation period to cover k-space were described. In these sequences, the total magnetization contained in the desired slice of tlie sample was flipped into tlie transverse plane and used over and over until all data points were acquired. In this section, sequences tliat use multiple excitation pulses are described. A common feature of these sequences is the use of low flip angle RF pulses so that only a fraction of the total magnetization is used in the k-space evolutíon along the read direction.

III.1 FLASH imaging sequence

Wlien small flip angles are used for selective excitation, the signal resulting from a flip angle 0 is proportional to $\sin\theta$, while tlie remaining longitudinal magnetization is proportional to $\cos\theta$. Therefore, it is possible to use a rapid succession of low-angle excitations to scan k-space entirely in a short period of time. This idea, due to Haase and co-workers[22], was termed Fast Low-Angle Shot (FLASH) imaging sequence. In this sequence a TR time short compared to T_1 is used. After n RF pulses of flip angle 0 the initial amplitude of the FID is $M_0 \cos^n\theta \sin\theta$. Typically θ is 5°. It is possible to trade-off imaging speed and SNR by adjusting θ and TR.

FLASH necessarily uses gradient refocusing since the use of 180° refocusing RF pulses causes unwanted disturbance of the stored longitudinal magnetization, and slows the imaging sequence down. Therefore, FLASH is subject to T_2^* relaxation. There is little intrinsic T_1 weighting in the FLASH sequence due to the very short TR (on the order of a few ms) used. Since

FLASH can be performed on time scales short compared to T_1, and T_2, it offers a vast number of possibilities for contrast manipulation that can not be achieved with conventional gradient-echo imaging. There are no intrinsic requirements in FLASH with respect to the acquisition window W or the eclio time TE, wliicli can be set arbitrarily according to the application. Such flexibility is not found in EPI, whose image quality decreases severely whenever the total image acquisition time approaches T_2^*.

A number of variations of the FLASH sequence were proposed. In Spoiled FLASH[23], a deliberate gradient spoiling pulse is applied at the end of each read period to suppress any remaining transverse coherence that might interfere with the next cycle. A higli-gradient version named Snapshot FLASH[24,25] enables images to be obtained in times on tlie order of 100 ms. Iii reference [24] Haase reported a sequence that used a TR of 3 ms and acquisition window of 1.6 ms for acquiring a 128 x 64 image in 192 ms. A disadvantage of using short acquisition windows is the increased noise component associated with the increased acquisition bandwidth. To prevent SNR degradation, the value of TR can be increased when sample motion is slow to compensate for the reduced bandwidtli.

111.2 **BURST** imaging sequence

The BURST Imaging sequence was originally developed by Hennig and Mueri[26] on a liigh-field animal scanner and later applied on a clinical whole body system[27]. In this sequence, a number N_p of very low flip-angle RF pulses is applied to tlie sample in tlie presence of a strong read gradient. The RF pulses are equally spaced so that by leaving tlie read gradient on after the last RF pulse, a string of N_p frequency encoded echoes will be generated. Phase encoding takes place by applying a constant gradient ortliogonal to the read gradient during the acquisition window W. For an isotropic FOV, the strength of the phase encoding gradient G_y is related to the strengtli of the read gradient G_x by $G_y = G_x/N_p$. Application of a phase-encoding gradient simultaneously with the read gradient leads to non-orthogonal sampling in k-space and therefore to errors in tlie reconstruction of the image by 2D Fourier transform. In particular, tlie image will be tilted by an angle $\theta = tan^{-1}(1/N_p)$, but this artifact can be neglected in practice for N_p sufficiently large. Considerable care has to be given to the choice of amplitude of the RF pulses. A severe artifact can be caused by unequal intensities of the echoes, leading to distortions iii tlie point-spread function for the image in the phase-encoding direction[27]. Therefore, the tip angle of the RF pulses has to be chosen so that the echo amplitudes remain as constant as possible. Usually the tip angle a of the RF pulses is chosen so that $\alpha N_p \approx 90°$. Several slice-selection schemes can be devised for the BURST imaging sequence[27]. The rnost common approach is to place a slice-selective refocusing 180° RF pulse between the train of low flip angle RF pulses and the echo train. This approach will be discussed bellow when the DUFIS imaging sequence is described.

Using tlie BURST sequence, images with a 64 x 64 data matrix have been acquired using an acquisition window W = 40 ms and a total time of 85 ms for completion of the entire sequence[27]. The BURST sequence was proposed as an alternative to the very rapid gradient switching required by EPI and the strong RF power deposition of FLASH and its variant sequences. In particular, the main advantages of BURST are that is does not require any gradient switching (and therefore iio hardware modifications) and has no RF power deposition concerns. However, the image resolution is far from the ones achieved by conventional MRI. The SNR in BURST is intrinsically poor due to the low signal amplitude of the echoes, and the large acquisition bandwidths used. Since the flip angle α of each pulse is smaller than 5°, the signal amplitude will be less than 10% of the equilibrium value[27]. Total acquisition tirnes are limited on the one hand by transmitter power concerns when faster acquisitions are desired, and by diffusion attenuation as well as T_2 decay of the signal on tlie other hand when longer acquisition times are desirable.

111.3 Dante ultra-fast imaging sequence (DUFIS)

The Dante Ultra-Fast Imaging Sequence (DUFIS) was proposed by Lowe and Wysong[28]. As main advantages, the sequence does not use any rapidly switched gradients, is insensitive to magnetic field inhomogeneities and does not require large RF power deposition, having no limitation on imaging speed other than

the receiver bandwidth and gradient strength. The major limitation of DUFIS, like in BURST, is found in the relatively poor SNR in comparison to conventional spin-echo MRI.

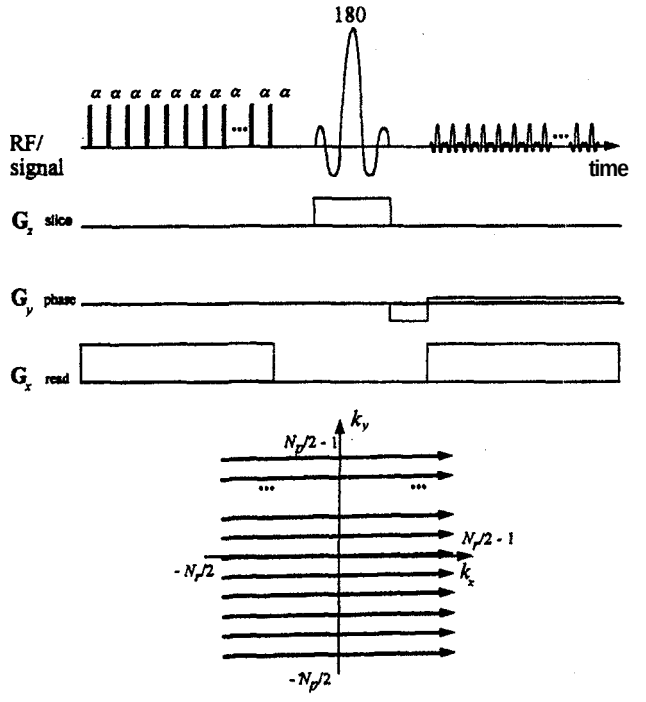

Figure 5. Dante Ultra-Fast Imaging Sequence (DUFIS). A string of N_p RF pulses of low flip- angle a is applied in the presence of a strong read gradient. The magnetization produced by this string of RF pulses is then refocussed by a slice-selective 180° RF pulse and phase-encoded to produce a train of N_p echoes, each echo corresponding to a different line in k-space. This sequence is also called BURST.

The DUFIS time diagram and k-space trajectories are described in Fig. 5. The sequence uses a string of N_p low flip-angle RF pulses to excite the sample in the presence of a read gradient. Each of the RF pulses is applied at times $0, \tau, 2\tau, \ldots, (N_p-1)\tau$ to produce a nutation angle a. After this string of RF pulses, spin-echoes (or gradient-echoes) spaced τ apart are generated using a 180° (or a gradient reversal), which in the absence of phase-encoding are identical in shape. Phase-encoding of the echoes can done using either a blipped gradient in a similar way to EPI or using a low-level constant gradient, as described in BURST. The use of a low-level constant phase-encoding gradient has the advantage of being less demanding on the gradient system, and the resulting non-orthogonal scan of k-space does not introduce any noticeable artifacts in the image. Slice-selection is achieved by using a 180° RF pulse in the presence of a slice-selective gradient, as shown in Fig. 5. Since there is no time gap between the echoes, this sequence enables the fastest possible imaging time for an imaging sequence that does not employ a simultaneous (multi-coil or phased array) detection scheme. DUFIS images of size 64 × 32 were taken using RF pulses of flip angles $\alpha = 3.2°$ spaced 200 μs apart in a total acquisition time of 16.9 ms [28].

111.4 Optimized ultra-fast imaging Sequence (OUFIS)

The RF pulse string used in BURST and in DUFIS to excite the sample is essentially a DANTE pulse train[29]. This pulse train is highly frequency selective, so that only narrow strips of the sample corresponding to approximately $1/N_p$ of the magnetization contained in an imaging voxel are excited. The magnetization between these strips is left unused, resulting low sensitivity and poor SNR. In addition, the RF flip angle a has to be restricted to $\alpha = 90°/N_p$ in order to avoid artifacts resulting from non-uniform echoes amplitude. For $N_p = 64$, $\alpha = 1.406°$, so that only a very small signal amplitude is obtained for each echo. An alternative way to excite the sample magnetization in a more efficient way is to use phase modulation of the DANTE sequence[30,31], so that more frequencies of the sample are excited and a larger flip angle can be used, for a combined overall improvement in SNR. By allowing the RF pulses in the DANTE train to have different phases, the SNR in BURST and DUFIS can be optimized. The resulting sequence is called OUFIS[32], for Optimized Ultra-Fast Imaging Sequence. By defining a sequence's performance measure in terms of an efficiency index e given by:

$$e = \sqrt{\sum_{i=1}^{N_r} A_i^2} \qquad (14)$$

the efficiency of a 64-pulse single phase DUFIS at its optimal flip angle $\alpha = 1.406°$ is $e = 14.4\%$. By allowing the individual low flip angle RF pulses to have phases different than 0°, the efficiency of this multi-phase OUFIS sequence jumps to e = 97.2%, a factor of 6.75 times larger than the single phase DUFIS sequence. The flip angle a of the RF pulses increases from $\alpha = 1.406°$ in DUFIS to a = 11.25° in OUFIS, a factor

of $\sqrt{N_p}$ larger for $N_p \simeq 64$ [32]. When the phase of the RF pulses is constrained to be either 0° or 180°, the efficiency of this two-phase OUFIS sequence is e = 93.3% at $\alpha = 11.25°$. Fig. 6 shows the time diagram for a two-phase OUFIS sequence. k-space trajectories are the same as in Fig. 5. The phase of the RF pulses can be optimized for best efficiency using either numerical[32] or analytical methods[33]. In particular, both numerical and analytical methods sliow that the maximum uniform signal amplitude of the echoes obtained from a string of N_p RF pulses is $M_0/\sqrt{N_p}$, where M_0 is the transverse magnetization amplitude produced by a single 90° RF pulse. In practice this gain of $\sqrt{N_p}$ in signal amplitude with respect to BURST and DUFIS is valid only for $N_p < 32$ RF pulses. For $N_p > 32$ there is an increasing saturation of the maximum echo amplitude due to nonideal excitation and diffusion effects[32,33]. A major disadvantage common to BURST, OUFIS and DUFIS is the long time the transverse magnetization spends under a strong read gradient. This leads to strong attenuation due to diffusion of the later echoes produced by the early RF pulse. For brain images, for example, the amplitudes of the last few echoes are only a small fraction of that of the first echo, which brings undesired blurring of the image in the phase-encoding direction. This problem can be addressed by breaking the sequence into smaller segments. For an image with 64 echoes, for example, the OUFIS sequence can be broken into 4 shots of 16 pulses each, or alternatively the 16 echoes produced by a single 16 pulse excitation period can be refocused 4 times to produce the 64 lines in *k*-space. This approach is called Segmented Hybrid/Multi-Shot OUFIS[34], and strongly alleviates the diffusion attenuation of the signal by avoiding the long exposure of the transverse magnetization to a fixed read gradient.

OUFIS can also be used in 3D experiments by acquiring successive 2D images of consecutive slices of the sample. Using this approach, 3D images of size 128 x 64 x 32 have been collected in 64 s with an effective TE of 46 ms and a TR of 2s [35]. Another approach for obtaining 3D information with BURST/DUFIS has been reportecl that takes advantage of the fact that single-phase RF pulses excite only narrow strips within a pixel. The approach consists of doing multiple 2D experiments and shifting the frequency of the RF pulses so that a different strip of a pixel is selected each time the 2D experiment is repeated. This approach was named Frequency-Shifted BURST MRI[36].

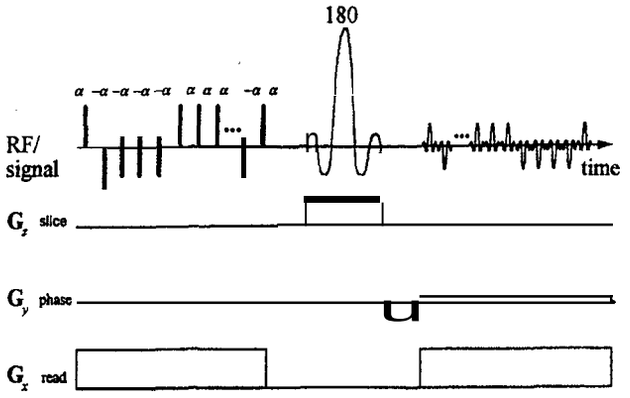

Figure 6. Optimized Ultra-Fast Imaging Sequence (OUFIS). This sequence optimizes the use of the magnetization in DUFIS/BURST by allowing the RF pulses of flip angle α to have either a 0° or a 180° phase in a pre-established order.

III.5 Rotating ultra-fast imaging sequence (RUFIS)

The approaches discussed so far for producing MR images utilize echoes that are frequency encoded along one direction of k-space and phase encoded in the orthogonal direction. Another way of obtaining an image is to use the FIDs generated by the RF pulses and to frequency encode them along different angular orientations in k-space. Each FID corresponds to a single radial line in k-space along the gradient's direction, and the image can be reconstructed using the Projection Reconstruction process. Such an approach is used in the Rotating Ultra-fast Imaging Sequence (RUFIS)[36–39]. As shown in Fig. 7, the technique consists of a rapid succession of N_p low flip angle RF pulses in the presente of a gradient that is rotated in steps. The duration of each RF pulse is sufficiently short that they still excite uniformly the entire region of interest. Each FID is acquired after the corresponding RF pulse and the gradient direction is rotated by a step of $\Delta\theta = \pi/N_p$ immediately after the FID is acquired and before the next RF pulse. Since changes in gradient between successive steps are small, no ramps are necessary. By using RUFIS, 32 × 32 images can be acquired in 8 ms [38], and the SNR is comparable to FLASH. One problem associated with the acquisition of FIDs is that the

time origin of each FID occurs during the application of the RF pulse and therefore can not be collected, but this time origin can be reconstructed by means of a robust mathematical technique.

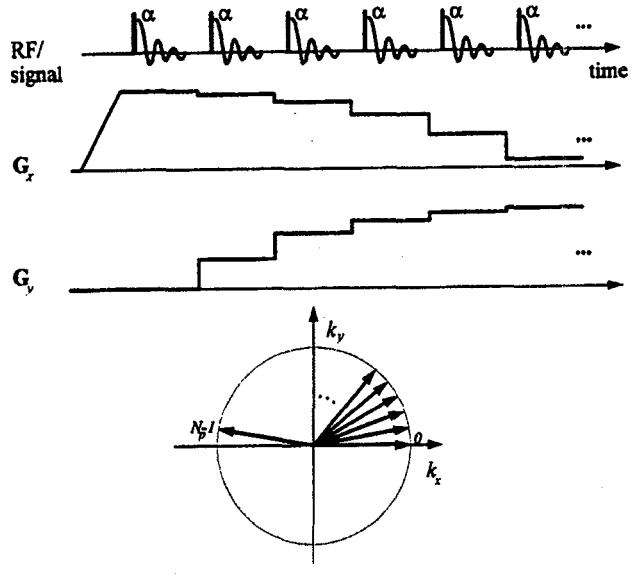

Figure 7. Rotating Ultra-Fast Imaging Sequence (RUFIS). Tliis sequence uses a string of low flip angle RF pulses to generate FIDs wliicli are acquired in tlie presence of a radial gradient. The direction of the gradient is stepped incrementally after the acquisition of eacli FID, resulting in a radial samplinR of k-space.

IV. Applications of ultra-fast MRI sequences

One of the main and most obvious applications of Ultra-Fast MRI sequences is found in processes affected by motion of the sample during the acquisition time. Since ultra-fast MR images can be collected in less than 100 ms, they are insensitive to patient motion, and to physiologicalmotion as well. In tlie gastroiiitestinal system, for example, conventional MR images are subject to artifacts caused by respiration and peristalsis[40,41]. While a number of different approaches can be used to reduce the intensity of motions artifacts, in particular respiratory gating[42], ordered phase encoding[43] and gradient moment nulling[44], ultra-fast MRI techniques can eliminate completely the artifacts caused by physiological motion. In particular, EPI lias been used to image the abdomen[45–47], and FLASH has been used for tlie same purpose together with breath-hold techniques[48].

Ultra-Fast MRI sequences inade it possible to image tlie heart, one of the most difficult to image moving organs of the body, without the need to gate the sequence to the cardiac cycle. This major advantage solves many of tlie problems encountered when imaging patients with cardiac arrhythmia. Rzedzian and Pykett were among the first to use EPI to image the heart[49]. Since then, MRI movies of the heart have been obtained using CINE techniques[50,51], and short and long-axis images of the heart are normally acquired using EPI[52].

Magnetic Resonance Angiograms[53–55] can be obtained using MRI. Recently, ultra-fast MRI sequences including FLASH[56], EPI[57] and Spiral-Scan[58] have been used for obtaining angiograms. Flow velocity images have been produced using Spiral-Scan[59] and DUFIS[60,61], while RUFIS has been used to image turbulent jets in stenotic phantoms[37–39], a metliod that lias large potential application in the diagnostics of cardiac and vascular diseases.

The study of organ functionality with MRI has been subject to large improvements with the use of ultra-fast MRI sequences. Using a number of techniques now called Functional MRI, brain function has been studied in terms of task activation and visual stimulation. Clianges in blood oxygenation[62,63] or in tissue regional perfusion[63,64] cause changes in the MRI signal that can be detected with an appropriate MRI sequence. The use of ultra-fast MRI sequences allowed for a higher temporal resolution to track the MRI signal following a particular stimulus of the brain[65–68].

Although research on ultra-fast imaging sequences started as early as in the late 1970's, there are still lots of developmental work to be done before these sequences become as commonly used as the slower forms of MRI. While tlie principles of obtaining an ultra-fast MR image appear to be well understood, there are still many experimental and hardware problems to be addressed in order to allow its implementation. However, tlie higlier temporal resolution achieved with ultra-fast MRI sequences lias greatly expanded the range of applications of MRI, and as these sequences become more available to clinical institutions, one might expect newer applications to appear. Besides providing a reduction in scan time (and therefore in costs) for tlie imaging protocols already in use, ultra-fast MRI is expected to play a major role in applications like inter-

ventional imaging, dynamic and functional studies and also in other applications such as flow ltinetics.

References

1. P. T. Callaghan, *Principles of Nuclear Magnetic Resonance Microscopy* (Oxford University Psess, Oxford, 1993).
2. P. Mansfield, J. Phys. C10, L55 (1977).
3. P. Mansfield and I. L. Pykett, J. Magn. Reson. 29, 355 (1978).
4. B. Chapman, R. Turner, R. J. Ordidge, M. Doyle, M. Cawley, R. Coxoii, P. Glover and P. Mansfield, Magn. Reson. Med. 5, 246 (1987).
5. R. J. Ordidge, A. Howseman, R. Coxon, R. Turner, B. Chapman, P. Glover, M. Stehling and P. Mansfield, Magn. Reson. Med. 10, 227 (1989).
6. R. R. Rzedzian and I. L. Pykett, Radiology 161(P), 338 (1986).
7. I, L. Pykett and R. R. Rzedzian, Magn. Reson. Med. 5, 563 (1987).
8. M. S. Cohen and R. M. Weisskoff, Magn. Reson. Irnag. 9, 1 (1991).
9. F. Farzaneh, S. J. Riederer and N. J. Pelc, Magn. Reson. Med. 14, 123 (1990).
10. P. Mansfield and B. Chapman, J. Phys. E: Sci. Instrum. 19, 540 (1986).
11. P. Mansfield and B. Chapman, J. Magii. Reson. 66, 573 (1986).
12. P. Mansfield and B. Chapman, J. Magn. Reson. 72, 211 (1987).
13. C. B. Ahn, J. H. Kim, and Z. H. Cho, EEE Trans. Med. Imag. MI-5, 2 (1986).
14. P. D. Gatehouse, D. N. Finnin, S. Collins and D. B. Longrriore, Magn. Reson. Med. 31, 504 (1994).
15. C. H. Meyer, B. S. Hu, D. G. Nishimura and A. Macovsky, Magn. Reson. Med. 28, 202 (1992).
16. G. H. Glover, A. T. Lee, C. H. Meyer, Proc. 12th Ann. Meeting SMRM, 197 (1993).
17. D. Nishimura, P. Irarrazabal, C. H. Meyer, Magn. Reson. Med. 33, 549 (1995).
18. E. Yudilevich and H. Stark, EEE Trans. Med. Imag. MI-6, 337 (1987).
19. D. C. Noll, C. H. Meyer, J. M. Pauly aiid D. G. Nishimura, EEE Trans. Med. Imag. 10, 629 (1991).
20. D. C. Noll, J. M. Pauly, C. H. Meyer, D. G. Nishimura and A. Macovsky, Magn. Reson. Med. 25, 319 (1992).
21. K. F. King, T. K. F. Foo and C. R. Crawford, Magn. Reson. Med. 34, 156 (1995).
22. A. Haase, J. Frahm, D. Matthaei, W. Hanicke and K. D. Merboldt, J. Magn. Reson. 67, 258 (1986).
23. J. Frahm, W. Hanicke and K. D. Merboldt, J. Magn. Reson. 72, 307 (1987).
24. A. Haase, Magn. Reson. Med. 13, 77 (1990).
25. A. Haase, D. Matthaei, R. Bartkowski, E. Duhmke and D. Leibfritz, J. Comput. Assisted Tomography 13, 1036 (1989).
26. J. Hermig and M. Mueri, Proc. 7th Ann. Meeting SMRM, 238 (1988).
27. J. Hennig and M. Hodapp, MAGMA 1, 39 (1993).
28. I. J. Lowe and R. E. Wysong, J. Magn. Reson., Series B 101, 106 (1993).
29. G. A. Morris and R. Freeman, J. Magn. Reson. 29, 433 (1978).
30. G. Bodenhausen, R. Freeman, and G. A. Morris, J. Magn. Reson. 23, 171 (1976).
31. P. Le Roux, J. Pauly and A. Macovski, Proc. 10th Ann. Meeting SMRM, 269 (1991).
32. L. Zha and I. J. Lowe, Magn. Reson. Med. 33, 377 (1995).
33. P. V. Gelderen, J. H. Duyn and C. T. W. Moonen, J. Magii. Reson.. Series B 107, 78 (1995).
34. L. Zha, A. C. Silva and I. J. Lowe, Proc. 2nd Ann. Meeting SMR, 1091 (1994).
35. S. L. Talagala, L. Zha and I. J. Lowe, Proc. 2nd Ann. Meeting SMR, 790 (1994).
36. D. P. Madio and I. J. Lowe, Proc. 2nd Ann. Meeting SMR, 471 (1994).
37. D. P. Madio and I. J. Lowe, Proc. 36th Exp. Nuclear Magn. Reson. Conf., 294 (1995).
38. D. P. Madio and I. J. Lowe, Proc. 3rd Ann. Meeting SMR, 420 (1995).
39. D. P. Madio and I. J. Lowe, Magn. Reson. Med., in press (1995).
40. M. L. Wood, V. M. Runge and R. M. Henkelman, Am. J. Roetgenol. 150, 513 (1988).
41. M. L. Wood and R. M. Henkelman, Med. Phys. 12, 143 (1986).
42. V. M. Runge, J. A. Clanton, C. L. Partain and A. E. James, Radiology 151, 521 (1984).

43. D. R. Bailes, D. J. Gilderdale, G. M. Bydder, A. G. Collins and D. N. Firmin, J. Comput. Assist. Tomogr. 9, 835 (1985).
44. P. M. Pattany, J. J. Philips, C. C. Lee, J. D. Lipcamon, J. L. Durek, J. M. McNally and S. N. Mohapatra, J. Assist. Comput. Tomogr. **11**(3), 369 (1987).
45. M. K. Stehling, D. F. Evans, Larnont, R. J. Ordidge, A. M. Howseman, B. Chapman, R. Coxon, P. Mansfield, J. D. Hardcastle and R. E. Coupland, Radiology 171, 41 (1989).
46. S. Saini, D. D. Stark, R. R. Rzedzian, I. L. Pyltett, E. Rumrneny, P. F. Hahn, J. Wittenberg and J. T. Ferrucci, Radiology 173, 111 (1989).
47. P. F. Hahn, S. Siani, M. S. Cohen et. al., Magn. Reson. Med. 25, 380 (1992).
48. E. C. Unger, M. S. Cohen, R. A. Gatenby, M. R. Clair, T. R. Brown, S. J. Nelson and J. S. McGlone, J. Comput. Assist. Tomogr. **12(4)**, 575 (1988).
49. R. R. Rzedzian and I. L. Pykett, Am. J. Roetgenol. 149, 245 (1987).
50. G. H. Glover and N. J. Pelc, In: H. Y. Kressel Proc. of the Magnetic resonance Annual Meeting 1988. New York, Raven, 1988) p. 299.
51. M. S. Cohen, R. M. Weisskoffand R. R. Rzedzian, Radiology **173(P)**, 359 (1989).
52. R. M. Weissltoff, M. S. Cohen and R. R. Rzedzian, Magn. Reson. Med. 29, 796 (1993).
53. C. L. Dumoulin and H. R. Hart, Radiology 161, 717 (1986).
54. G. A. Laub and W. A. Kaiser, J. Comput. Assist. Tomogr. **12(3)**, 377 (1988).
55. C. L. Dumoulin, S. P. Souza, M. F. Wallíer and W. Wagle, Magn. Reson. Med. 9, 139 (1989).
56. D. J. Atkinson and R. R. Edelman, Radiology 178, 357 (1991).
57. D. N. Firmin, R. H. Klipstein, G. L. Hounsfield, M. P. Paley and D. B. Longmore, Magn. Reson. Med. 12, 316 (1989).
58. C. H. Meyer, B. S. Hu, D. G. Nishimura and A. Macovslty, Magn. Reson. Med. 28, 202 (1992).
59. G. B. Pilíe, C. H. Meyer, T. J. Brosnan and N. J. Pelc, Magn. Reson. Med. 32, 476 (1994).
60. R. Wysong and I. J. Lowe, Proc. 12th Ann. Meeting SMRM, 646 (1993).
61. D. P. Madio, R. Wysong and I. J. Lowe, Proc. 12th Ann. Meeting SMRM, 647 (1993).
62. S. Ogawa. T.-M. Lee, A. S. Nayak and P. Glynn, Magn. Reson. Med. 14, 68 (1990).
63. K. K. Kwong, J. W. Belliveau, D. A. Chesler, I. E. Goldberg, R. M. Weisskoff, B. P. Poncelet, D. N. Kennedy, B. E. Hoppel. M. S. Cohen, R. Tumer, H.-M. Cheng, T. J. Brady and B. R. Rosen, Proc. Natl. Acad. Sci. USA 89, 5675 (1992).
64. A. C. Silva, W. Zhang, D. S. Williarns and A. P. Koretsky, Magn. Reson. Med. 33, 209 (1995).
65. J. W. Belliveau, D. N. Kennedy, R. C. McKinstry, B. R. Buchbinder, R. M. Weisslroff, M. S. Cohen, J. M. Vevea, T. J. Brady and B. R. Rosen, Science 254, 716 (1991).
66. P. A. Bandettini, E. C. Wong, R. S. Hinks, R. S. Tikofsky and James S. Hyde, Magn. Reson. Med. 25, 390 (1992).
67. R. Turner, P. Jezzard, H. wen, K. K. Kwong, D. Le Bihan, T. Zeffiro and R. S. Balaban, Magn. Reson. Med. 29, 277 (1993).
68. M. S. Cohen, B. R. Rosen and T. J. Brady, MR, Winter 1992.